

RESEARCH ARTICLE | AUGUST 15 2025

Valence photoelectron spectra of thiouracils in the gas phase

Dennis Mayer ; Evgenii Titov ; Fabiano Lever ; Lisa Mehner ; Marta L. Murillo-Sánchez ; Constantin Walz ; John Bozek ; Peter Saalfrank ; Markus Gühr 



J. Chem. Phys. 163, 074301 (2025)

<https://doi.org/10.1063/5.0279536>



View
Online



Export
Citation

Articles You May Be Interested In

X-ray photoelectron and NEXAFS spectroscopy of thionated uracils in the gas phase

J. Chem. Phys. (October 2024)

Electron propagator and coupled-cluster calculations on the photoelectron spectra of thiouracil and dithiouracil anions

J. Chem. Phys. (February 2011)

Photoelectron spectroscopic study of the negative ions of 4-thiouracil and 2,4-dithiouracil

J. Chem. Phys. (February 2011)

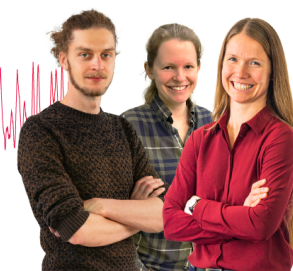
Webinar From Noise to Knowledge

May 13th – Register now



Zurich
Instruments

Universität
Konstanz



Valence photoelectron spectra of thiouracils in the gas phase

Cite as: J. Chem. Phys. 163, 074301 (2025); doi: 10.1063/5.0279536

Submitted: 7 May 2025 • Accepted: 24 July 2025 •

Published Online: 15 August 2025



Dennis Mayer,^{1,a)} Evgenii Titov,^{2,a)} Fabiano Lever,¹ Lisa Mehner,³ Marta L. Murillo-Sánchez,⁴ Constantin Walz,³ John Bozek,⁵ Peter Saalfrank,^{2,3} and Markus Gühr^{1,6}

AFFILIATIONS

¹ Deutsches Elektronen-Synchrotron DESY, Notkestr. 85, 22607 Hamburg, Germany

² Institut für Chemie, Universität Potsdam, Karl-Liebknecht-Str. 24/25, 14476 Potsdam, Germany

³ Institut für Physik und Astronomie, Universität Potsdam, Karl-Liebknecht-Str. 24/25, 14476 Potsdam, Germany

⁴ Max-Planck-Institut für Kernphysik, Saupfercheckweg 1, 69117 Heidelberg, Germany

⁵ Synchrotron SOLEIL, L'Orme de Merisiers, Départementale 128, 91190 Saint-Aubin, France

⁶ Institut für Physikalische Chemie, Universität Hamburg, Grindelallee 117, 20146 Hamburg, Germany

^{a)} Authors to whom correspondence should be addressed: dennis.mayer@desy.de and titov@uni-potsdam.de

ABSTRACT

We present a combined experimental and theoretical study of the vibrationally resolved valence photoelectron spectra of the complete series of thiouracils (2-thiouracil, 4-thiouracil, and 2,4-dithiouracil) for binding energies between 8 and 17 eV. The theoretical spectra were calculated using equation-of-motion coupled cluster theory for ionization potential combined with the time-independent double-harmonic adiabatic Hessian approach. For all three thiouracils, the first ionization potential is found between 8.4 and 8.7 eV, which is 1 eV lower than for the canonical nucleobase uracil. Ionization bands up to 12 eV show strong vibrational progressions and are well reproduced by the calculations. These bands are attributed to the ionization of (primarily) sulfur- and oxygen-localized valence molecular orbitals. For higher binding energies, the calculations indicate that nonadiabatic couplings are important for the interpretation of the photoelectron spectra.

© 2025 Author(s). All article content, except where otherwise noted, is licensed under a Creative Commons Attribution (CC BY) license (<https://creativecommons.org/licenses/by/4.0/>). <https://doi.org/10.1063/5.0279536>

INTRODUCTION

Thionated nucleobases have a long history as medical drugs, e.g., as immunosuppressants or photosensitizers in photodynamic therapy.^{1,2} This is due to their similarity to canonical nucleobases, allowing for substitution in organic tissue, and their significantly altered behavior upon excitation with ultraviolet light. The substitution of oxygen by sulfur increases the spin-orbit coupling in the molecules, leading to an increased population of long-lived triplet states.^{1,2} In these states, radical formation or dimerization may occur, potentially altering DNA strands and their behavior, which can lead to cell death.^{3,4}

In recent years, the photodynamics of thiouracils, as one of the simplest thionucleobase classes, has gained considerable attention. Different spectroscopy techniques have been employed to unravel

the relaxation pathway toward the triplet states, ranging from ultrafast transient absorption^{5–9} to ion and electron spectroscopy from the UV to soft x rays.^{10–15} In particular, the charged particle experiments, which were conducted in the gas phase, were often referenced to solution-phase spectra or did not have well-resolved ground-state reference spectra to begin with. Recently, some authors have started to close these gaps for thiouracils by measuring gas-phase references for the UV and x-ray absorption as well as x-ray photoelectron spectra, which were combined with state-of-the-art quantum chemical calculations.^{16,17} In the light of time-resolved valence photoelectron spectra performed in the group of Ullrich^{9,11,12} and simulations of these spectra by Ruckebauer *et al.*,¹⁸ we identify a lack of a complete set of high-resolution reference valence photoelectron spectra.

In this contribution, we present the static VUV photoelectron spectra of the three molecules, 2-thiouracil and 4-thiouracil

(2-TU and 4-TU), as well as 2,4-dithiouracil (2,4-dTU), measured at the PLEIADES beamline of the synchrotron SOLEIL. The experimental spectra are discussed with the help of coupled cluster calculations in order to understand the origins of the individual bands as well as observed vibrational progressions. Both the experiment and the calculations are also compared to previous studies on the molecules and studies on their canonical counterpart, uracil.

METHODS

Experimental details

The experiment was performed at the PLEIADES beamline of synchrotron SOLEIL.¹⁹ For sample delivery, a heatable gas cell was used inside the main vacuum chamber. The samples were heated up to 120 °C to achieve sufficient vapor pressure ($\sim 1 \times 10^{-4}$ mbar).²⁰ The main chamber pressure was kept at 1×10^{-7} mbar by means of differential pumping. The pressure inside the gas cell could not be measured but was expected to be between the main chamber pressure and the vapor pressure of the sample.

An Apple II HU 80 permanent magnet undulator was used to generate the VUV beam, and a 600 lines/mm grating was employed to select the final photon energy of 100 eV. The beam can enter and exit the gas cell through 10 mm long differential pumping tubes of 2 mm diameter. The focused beam size was about $100 \times 75 \mu\text{m}$,² where the vertical dimension is typically an image of the monochromator slit. The flux at the given photon energy was on the order of 1.2×10^{13} photons/s for a $75 \mu\text{m}$ monochromator slit. The monochromator slit size corresponds to a resolution of ~ 20 meV at a photon energy of 100 eV.

Electrons generated by the photon beam exited the gas cell through a slit facing the entrance of the hemispherical electron kinetic energy analyzer (Scienta R4000). The electron spectra were calibrated using a water signal from an initially hydrated sample. The pass energy was chosen such that the overall resolution was estimated to be 30 meV for the measurements.

Computational details

Geometry optimizations of the ground state of the neutrals were done at the coupled cluster singles and doubles (CCSD)²¹ level, whereas equation-of-motion CCSD for ionization potential (EOM-IP-CCSD)^{22,23} was used for the ground and excited states of the cations. No symmetry restrictions were applied. First, the polarized split-valence 6-31G* basis set^{24–26} was employed in these calculations. The located minimum energy structures were reoptimized using the triple-zeta cc-pVTZ basis set.^{27,28} The vibrational frequencies were calculated numerically using the 6-31G* basis set at the (EOM-IP-)CCSD/6-31G* optimized geometries. The calculations were performed with the Q-Chem 4.4 program.²⁹

The adiabatic ionization energies were calculated at the (EOM-IP-)CCSD/cc-pVTZ level and further corrected with zero point energies obtained at the (EOM-IP-)CCSD/6-31G* level to obtain the 0–0 energies (energy differences between the lowest vibrational states of the S_0 and D_i electronic states). We note that test calculations demonstrated very minor differences when using the cc-pVDZ frequencies instead of the 6-31G* frequencies. The EOM-IP-CCSD calculations of the (numerical) frequencies with the cc-pVTZ basis set are too demanding.

The vibrationally resolved photoelectron spectra were computed with the ezSpectrum 3.0 program.^{30,31} They were obtained using the time-independent double-harmonic adiabatic Hessian approach.³² The frequency alteration and Duschinsky rotations were taken into account. Up to two vibrational quanta were included for the initial (S_0) state and up to five in the final (D_i) states. The spectra were calculated at a temperature of 120 °C (393.15 K). The intensity threshold was set to 10^{-6} . The vibronic stick spectra $\{E_j, I_j\}$ were broadened with Lorentzians as

$$I(E) = \sum_j I_j \frac{\gamma^2}{(E - E_j)^2 + \gamma^2}$$

with $\gamma = 0.02$ eV. Here, E_j and I_j are the vibronic excitation energies and corresponding intensities, respectively.

The vertical electronic spectra were calculated using EOM-IP-CCSD/cc-pVTZ at the CCSD/cc-pVTZ optimized geometries. The intensities of the transitions were estimated as the product of left and right Dyson orbital norms.³³ The Dyson orbitals (and their norms) were calculated using Q-Chem 4.4.

RESULTS AND DISCUSSION

Experimental valence spectra

We start with the discussion of the experimental spectra. Figure 1 shows the valence photoelectron spectra of 2-thiouracil and 4-thiouracil (2-TU and 4-TU) as well as 2,4-dithiouracil (2,4-dTU) alongside the theoretical results. For comparison, a uracil spectrum is also shown in panel (a), with the experimental spectrum taken from Fulfer *et al.*³⁴ No background has been subtracted from the spectra, as after careful comparison with reference spectra of usual contaminations (i.e., N_2 and H_2O), we found that any background should be negligible. The measured electron kinetic energy window (80–95 eV) was in a range where the transmission function of the hemisphere is flat. Thus, no further normalization was done on the spectra.

The first ionization band has its first maximum at energies of 8.75 eV for 2-TU and 8.42 and 8.45 eV for 4-TU and 2,4-dTU, respectively. For 2-TU, this energy is in agreement with previous literature.^{10,35} In all three molecules, this first band shows some structure, indicating vibrational excitations. Compared to the canonical nucleobase uracil, the band is shifted on average by 0.9 eV toward lower binding energies upon thionation.^{34,36,37} The first ionization potentials found in this work, as well as the literature values, are summarized in Table I.

A second band appears at 9.98 and 9.83 eV for 2-TU and 4-TU, respectively, which are followed by a strong vibrational progression. In the case of 2-TU, the following three identifiable peaks are separated by ~ 0.22 eV. For 4-TU, the vibrationally resolved band reaches from 10.3 to 11.5 eV, covering ~ 5 peaks separated by ~ 0.2 eV. Interestingly, 2,4-dTU does not show any feature in the range between 9.5 and 11.5 eV. However, as mentioned above, the first valence band of uracil falls into the same energy range. This indicates that the second band might be associated with orbitals localized at the oxygen atom, as the absence of oxygen is what distinguishes 2,4-dTU from the other three molecules. In addition, the separation of the peaks in 2-TU and 4-TU (0.20–0.22 eV or 1600–1800 cm^{-1}) is similar to the frequency of the C=O bond stretch. As a consequence, one might

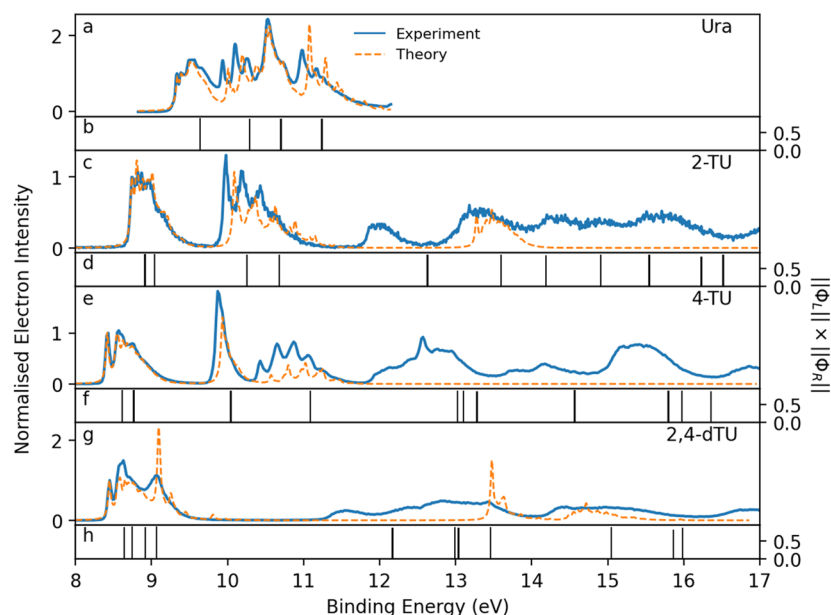


FIG. 1. Experimental (solid, blue line) taken at $h\nu = 100$ eV together with theoretical (dashed, orange line) photoelectron spectra for uracil (a) and the three thiouracils [(c), (e), and (g)] together with vertical excitation (stick) spectra [(b), (d), (f), and (h)]. Shifts of 0.05, 0.1, -0.02 , and -0.07 eV were applied to the theoretical spectra of Ura, 2-TU, 4-TU, and 2,4-dTU, respectively, to match the experimental spectra. The experimental uracil spectrum was taken from Fulfer *et al.*³⁴ at a photon energy of 40 eV.

assume that the first band in each of the three thionated molecules can be attributed to orbitals localized at the sulfur atom. The assignment to the atoms is verified by our theoretical calculations, which are discussed in the sections titled Vertical electronic transitions and Vibronic transitions.

Beyond 11.5 eV, more bands are visible; however, they are not structured as the first two. For 2-TU, a band around 12 eV is observed, followed by a broadband between 12.6 and 16.5 eV, which shows smaller peaks at ~ 13.1 , 14.2, 14.9, and 15.5 eV. 4-TU shows a broader band between 11.9 and 13.2 eV with a distinct peak at ~ 12.5 eV. This band is followed by two smaller peaks around 13.8 and 14.2 eV. Another band ranges between 15 and 16 eV with no distinct peak. The doubly thionated uracil shows a broad band between 11.3 and 13.8 eV with small peaks at around 11.5, 12.4, 12.8, and 13.4 eV. Another band appears between 14.2 and 16 eV with smaller peaks around 14.4 and 16 eV.

Vertical electronic transitions

The vertical ionization potentials and dominant Hartree-Fock canonical molecular orbitals (and their energies) involved in ionization are shown in Tables II, III, and IV for 2-TU, 4-TU, and 2,4-dTU, respectively. In agreement with Ruckebauer *et al.*,¹⁸ we find that the lowest energy band in the vibrationally resolved

spectrum stems from transitions solely to D_0 and D_1 for both 2-TU and 4-TU, whereas for 2,4-dTU it originates from the lowest four transitions, to D_0 – D_3 states. The corresponding molecular orbitals are dominated by n or π type contributions of sulfur.

Interestingly, for 2-TU, the leading orbital number in column 3 is monotonically decreasing, showing that the lowest state (D_0) corresponds to ionization from the HOMO (Highest Occupied Molecular Orbital), the next state (D_1) to HOMO-1, D_2 to HOMO-2, and so on, in agreement with Koopmans' theorem. In contrast, this is different for 4-TU and 2,4-dTU. For example, D_0 of 4-TU arises from HOMO-1, whereas D_1 arises from HOMO. The same is observed for 2,4-dTU. We note that in these cases, the energy gaps between both multi-electron states (D_0/D_1) and orbitals (HOMO/HOMO-1) are small, ~ 0.1 to 0.2 eV.

The D_2 and D_3 states of 2-TU and 4-TU correspond predominantly to ionization from oxygen (again, either from n or π type oxygen orbitals; see Tables II and III) with some contribution of the ring and the sulfur atom. This explains the lack of electronic transitions in the associated energy range (~ 10 to 11 eV) for 2,4-dTU, which does not contain oxygen.

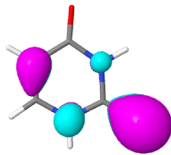
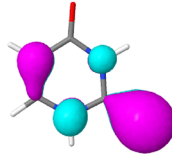
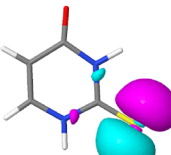
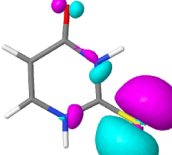
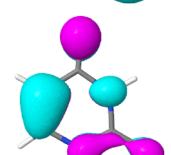
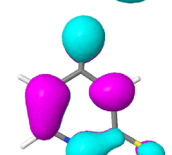
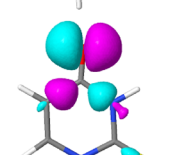
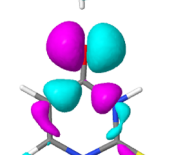
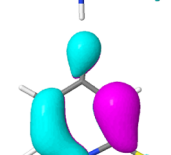
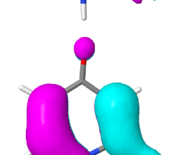
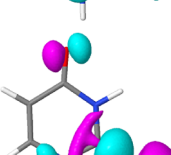
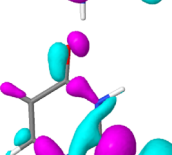
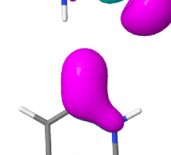
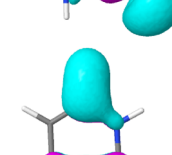
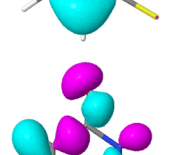
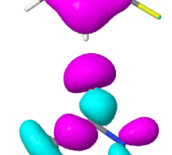
The first four transitions of all the molecules originate from ionization of the four highest molecular orbitals (HOMO to HOMO-3). The higher energy states correspond to ionization from lower orbitals, which often are dominated by a ring contribution, but in some cases also involve oxygen and/or sulfur atoms (see Tables II–IV).

It is instructive to note that Koopmans' ionization potentials, calculated as minus energies of respective leading molecular Hartree-Fock (canonical) orbitals, are overestimated by 0.2–2.3 eV with respect to the EOM-IP-CCSD values (compare columns 2 and 4 of Tables II–IV). In particular, the maximal and minimal deviations are 0.36 and 2.11 eV for 2-TU, 0.22 and 2.33 for 4-TU, and 0.30 and

TABLE I. Experimental ionization energies in eV for the three thiouracils and uracil.

	2-TU	4-TU	2,4-dTU	Ura
This work	8.74 ± 0.03	8.42 ± 0.01	8.45 ± 0.01	...
Literature	8.70^{10}	9.3^{34}
	8.80^{35}	9.46^{36}
				9.56^{37}

TABLE II. Vertical ionization potentials (calculated using EOM-IP-CCSD/cc-pVTZ and Koopmans' theorem) and molecular orbitals (canonical and Dyson) involved in ionization for the lowest eleven transitions of 2-TU. Orbital energies refer to Hartree–Fock. The HOMO is orbital no. 33.

Transition	Excitation energy (eV)	Leading orbital (contribution)	Minus orbital energy (eV)	Picture of the canonical orbital	Picture of the Dyson orbital
$S_0 \rightarrow D_0$	8.814	33(0.93)	9.170		
$S_0 \rightarrow D_1$	8.938	32(0.93)	9.497		
$S_0 \rightarrow D_2$	10.158	31(0.88)	10.857		
$S_0 \rightarrow D_3$	10.579	30(0.89)	12.517		
$S_0 \rightarrow D_4$	12.528	29(0.86)	13.551		
$S_0 \rightarrow D_5$	13.499	28(0.90)	14.803		
$S_0 \rightarrow D_6$	14.084	27(0.88)	15.592		
$S_0 \rightarrow D_7$	14.807	26(0.80)	16.653		

18 August 2025 06:58:52

TABLE II. (Continued.)

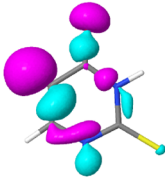
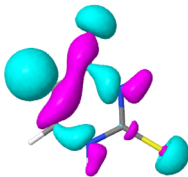
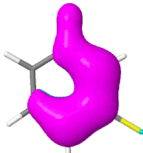
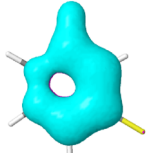
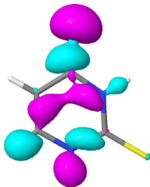
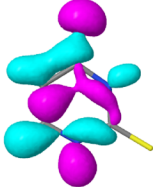
Transition	Excitation energy (eV)	Leading orbital (contribution)	Minus orbital energy (eV)	Picture of the canonical orbital	Picture of the Dyson orbital
$S_0 \rightarrow D_8$	15.445	25(0.78)	17.143		
$S_0 \rightarrow D_9$	16.132	24(0.86)	18.096		
$S_0 \rightarrow D_{10}$	16.417	23(0.84)	18.531		

TABLE III. Vertical ionization potentials (calculated using EOM-IP-CCSD/cc-pVTZ and Koopmans' theorem) and molecular orbitals (canonical and Dyson) involved in ionization for the lowest eleven transitions of 4-TU. The HOMO is orbital 33.

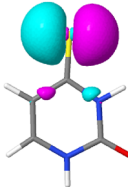
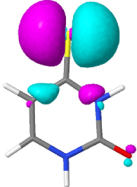
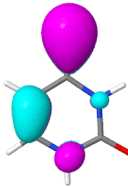
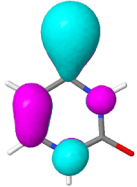
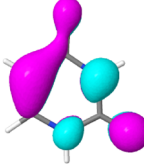
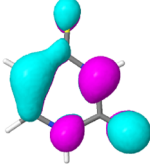
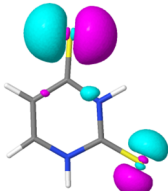
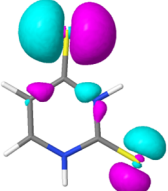
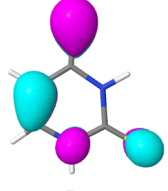
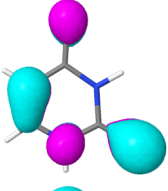
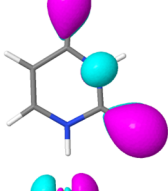
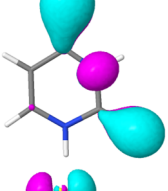
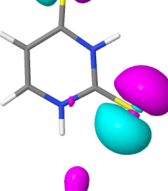
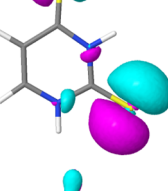
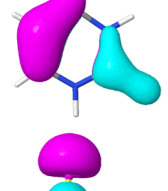
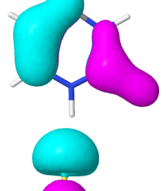
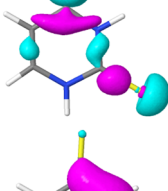
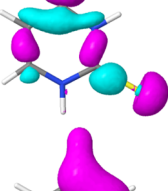
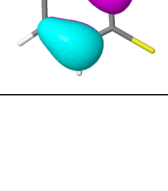
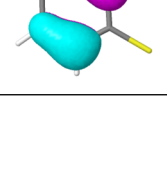
Transition	Excitation energy (eV)	Leading orbital (contribution)	Minus orbital energy (eV)	Picture of the canonical orbital	Picture of the Dyson orbital
$S_0 \rightarrow D_0$	8.635	32(0.93)	9.225		
$S_0 \rightarrow D_1$	8.786	33(0.93)	9.007		
$S_0 \rightarrow D_2$	10.062	31(0.91)	10.857		

TABLE III. (Continued.)

Transition	Excitation energy (eV)	Leading orbital (contribution)	Minus orbital energy (eV)	Picture of the canonical orbital	Picture of the Dyson orbital
$S_0 \rightarrow D_3$	11.106	30(0.88)	13.007		
$S_0 \rightarrow D_4$	13.043	27(0.83)	14.613		
$S_0 \rightarrow D_5$	13.119	28(0.88)	14.449		
$S_0 \rightarrow D_6$	13.299	29(0.80)	14.395		
$S_0 \rightarrow D_7$	14.585	26(0.90)	16.218		
$S_0 \rightarrow D_8$	15.818	24(0.66)	18.150		
$S_0 \rightarrow D_9$	15.997	25(0.66)	17.715		
$S_0 \rightarrow D_{10}$	16.376	23(0.87)	18.368		

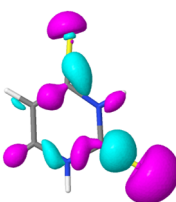
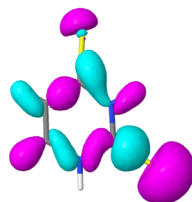
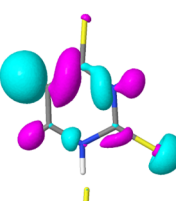
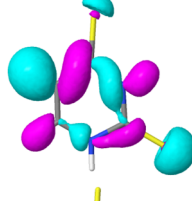
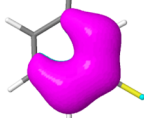
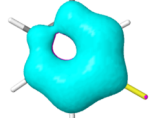
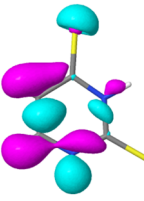
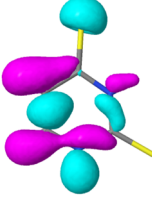
18 August 2025 06:58:52

TABLE IV. Vertical ionization potentials (calculated using EOM-IP-CCSD/cc-pVTZ and Koopmans' theorem) and molecular orbitals (canonical and Dyson) involved in ionization for the lowest eleven transitions of 2,4-dTU. The HOMO is orbital 37.

Transition	Excitation energy (eV)	Leading orbital (contribution)	Minus orbital energy (eV)	Picture of the canonical orbital	Picture of the Dyson orbital
$S_0 \rightarrow D_0$	8.713	36(0.92)	9.361		
$S_0 \rightarrow D_1$	8.815	37(0.86)	9.116		
$S_0 \rightarrow D_2$	8.989	35(0.84)	9.442		
$S_0 \rightarrow D_3$	9.137	34(0.92)	9.769		
$S_0 \rightarrow D_4$	12.238	33(0.90)	12.871		
$S_0 \rightarrow D_5$	13.062	32(0.91)	14.313		
$S_0 \rightarrow D_6$	13.107	31(0.88)	14.776		

18 August 2025 06:58:52

TABLE IV. (Continued.)

Transition	Excitation energy (eV)	Leading orbital (contribution)	Minus orbital energy (eV)	Picture of the canonical orbital	Picture of the Dyson orbital
$S_0 \rightarrow D_7$	13.526	30(0.90)	14.857		
$S_0 \rightarrow D_8$	15.116	29(0.90)	16.817		
$S_0 \rightarrow D_9$	15.935	27(0.84)	18.123		
$S_0 \rightarrow D_{10}$	16.052	28(0.89)	17.932		

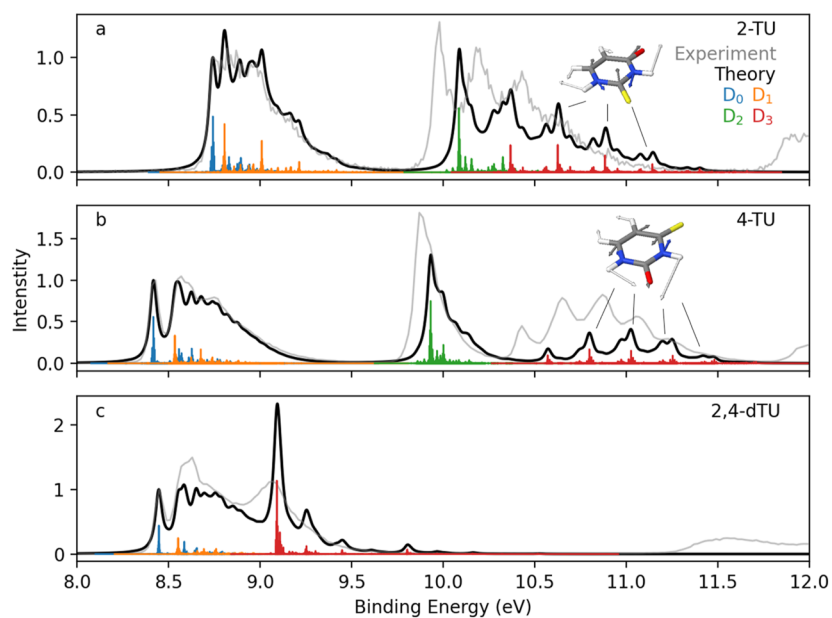


FIG. 2. Vibrationally resolved spectra between 8 and 12 eV. The contributions of the different cationic states to the theoretical spectrum (black) are colored (D_0 : blue, D_1 : orange, D_2 : green, and D_3 : red). The insets for 2-TU and 4-TU show the most prominent vibrational mode for the $S_0 \rightarrow D_3$ transition. The other vibronic transitions contributing to the spectrum are shown in Appendix A. The experimental spectra are shown in gray. The same shifts as in Fig. 1 have been applied to the theoretical spectra.

2.19 eV for 2,4-dTU. This clearly shows the limitation of a simple one-electron picture based on HF orbitals.

We have also calculated the Dyson orbitals for the S_0 – D_3 transitions. As shown in Tables II–IV, they are (very) similar to the corresponding canonical Hartree–Fock orbitals for all considered transitions (compare the last two columns of Tables II–IV).

Finally, we note that the Dyson orbital norms (presented in Fig. 1) are all rather large (left and right norms separately >0.9 , and their products >0.8) for the lowest eleven EOM-IP-CCSD transitions for all thionated molecules. This is in contrast to Ruckebauer *et al.*,¹⁸ where some transitions possess close-to-zero Dyson orbital norms (see the supplementary material of Ref. 18). We attribute this discrepancy to the use of different methods, EOM-IP-CCSD here vs MRCIS in Ref. 18.

Vibronic transitions

To calculate vibronic transitions, we applied the time-independent adiabatic Hessian approach, which requires geometry optimizations for both initial (S_0 in our case) and final (D_i in our case) states and the normal modes and vibrational frequencies for both states. We attempted to optimize D_0 – D_{10} states for each thionated molecule using EOM-IP-CCSD (and S_0 using CCSD). For uracil, only states D_0 – D_3 were optimized, corresponding to the energy range of the experimental spectrum of Fig. 1(a).

For all thionated molecules, we were able to optimize D_0 – D_4 (and S_0) states with the exception of D_2 for 2,4-dTU. Optimizations of higher lying cationic states often led to crossing regions (with a lower energy state) instead of zero-gradient minima of the states being optimized. This was also observed in the D_2 optimizations for 2,4-TU. However, the minima of the following higher energy states were located: D_5 for 2-TU, D_8 for 4-TU, and D_7 and D_8 for 2,4-dTU.

For the successfully optimized states, the vibrationally resolved spectra were calculated as Franck–Condon factors weighted with temperature-dependent coefficients according to the Boltzmann distribution. The stick spectra were concatenated and broadened with Lorentzians (see the section titled Methods) to obtain the total vibrationally resolved spectra shown in Fig. 1.

The vibronic stick spectra for the transitions to D_0 – D_3 are shown in Fig. 2, and assignments of the major vibronic transitions are provided in Appendix A (Figs. 3–16 and Tables V–XVIII). We note that the time-independent approach to calculate vibronic spectra (used in this work) provides direct information on which normal modes contribute to which transitions. The 0–0 transitions are the most intense for almost all considered cases. However, for the D_3 state of 4-TU, the most intense stick transition corresponds to excitation of mode 26 (NH bending + CO stretch + CC stretch; see Appendix A, Fig. 12). For the D_3 state of 2-TU, this transition (excitation of mode 26) is similar in intensity to the 0–0 transition (see Appendix A, Fig. 7). Further excitations of mode 26 (adding more vibrational quanta) are responsible for the observed progression of the $S_0 \rightarrow D_3$ transition in 4-TU and 2-TU (at ~ 10 to 11 eV in the experimental spectra of Figs. 1 and 2). The D_3 intensity for the 2,4-dTU is largely overestimated compared to the experimental spectrum.

The D_4 optimized geometries are considerably non-planar (in contrast to the D_0 – D_3 geometries), and the calculated Franck–Condon factors are very small for the $S_0 \rightarrow D_4$ transitions of

all three molecules (see Fig. 17 of Appendix B). The same was also observed for the D_8 state of 4-TU.

The optimized geometries of the D_5 state of 2-TU and the D_7 and D_8 states of 2,4-dTU are, in turn, planar, and the resulting Franck–Condon factors are relatively large. At that, the D_7 intensity is strongly overestimated in comparison to the experiment (Fig. 1).

Finally, we note that inclusion of nonadiabatic couplings (multistate treatment) seems to be necessary to properly describe the higher energy part of the spectra,^{38,39} because the undertaken geometry optimizations for higher energy cationic excited states usually hit intersection regions, suggesting the importance of the latter. To account for the nonadiabatic effects, one could attempt to construct a vibronic Hamiltonian and either diagonalize it or perform quantum dynamics simulations to eventually calculate the photoelectron spectra^{38–40} (which goes beyond the double-harmonic adiabatic Hessian approach). However, this is beyond the scope of the present work.

CONCLUSION

In this study, we reported the vibrationally resolved gas-phase valence photoelectron spectra of three thiouracils up to 17 eV. The data for 2-TU are in agreement with previously published results; the spectra for 4-TU and 2,4-dTU are presented for the first time to the best of our knowledge. The direct comparison of the three spectra in combination with the photoelectron spectrum of uracil allowed us to assign the first emerging band to the ionization of sulfur-dominated orbitals and the second band in 2- and 4-TU to oxygen-dominated orbitals. EOM-IP-CCSD calculations confirmed the assignment. The calculations were further combined with the time-independent double-harmonic adiabatic Hessian approach to simulate the vibrational progression of the ionization band. This resulted in a good match between theory and experiment for the first two ionization bands and allowed insight into the vibrational modes visible in the spectra. However, this approach fails to reproduce the bands for higher cationic states of the molecules. This is likely due to a missing treatment of nonadiabatic couplings between higher energy states.

ACKNOWLEDGMENTS

The spectra were recorded at the PLEIADES beamline at the synchrotron SOLEIL, France, under proposals 20200549 and 20211636. We acknowledge SOLEIL for the provision of synchrotron radiation facilities, and we would like to thank E. Robert and C. Nicolas for their technical assistance during the beamtime at PLEIADES. We thank BMBF for the funding via Verbundforschungsprojekt 05K19IP1. We acknowledge DFG funding via grants GU 1478/1-1 (M.G.) and SA 547/17-1 (P.S.) via the common project 445713302. We thank the Deutsche Forschungsgemeinschaft (DFG, German Research Foundation) for the financial support via CRC/SFB 1636 – Project ID 510943930 – Project Nos. A03 and B05.

AUTHOR DECLARATIONS

Conflict of Interest

The authors have no conflicts to disclose.

Author Contributions

Dennis Mayer: Data curation (equal); Formal analysis (equal); Investigation (equal); Validation (equal); Visualization (equal); Writing – original draft (equal); Writing – review & editing (equal). **Evgenii Titov:** Data curation (equal); Formal analysis (equal); Investigation (equal); Methodology (lead); Software (lead); Validation (equal); Visualization (equal); Writing – original draft (equal); Writing – review & editing (equal). **Fabiano Lever:** Investigation (equal); Writing – review & editing (equal). **Lisa Mehner:** Investigation (equal); Writing – review & editing (equal). **Marta L. Murillo-Sánchez:** Investigation (equal); Writing – review & editing (equal). **Constantin Walz:** Investigation (equal); Writing – review & editing (equal). **John Bozek:** Investigation (equal); Resources (equal); Writing – review & editing (equal). **Peter Saalfrank:** Funding acquisition (equal); Project administration (equal); Resources (equal); Supervision (equal); Writing – review & editing (equal). **Markus Gühr:** Conceptualization (lead); Funding acquisition (equal); Investigation (equal); Project administration (equal); Supervision (equal); Writing – review & editing (equal).

DATA AVAILABILITY

The experimental raw data were generated at the Synchrotron SOLEIL. Derived data and the simulated results supporting the findings of the study are openly available in Zenodo at <https://www.doi.org/10.5281/zenodo.15720936>.

APPENDIX A: ASSIGNMENT OF MAJOR VIBRONIC TRANSITIONS

The vibronic transitions shown in Fig. 2 are listed here in more detail. Figure 3 shows the vibronic stick spectra for 2-TU and the resulting electron spectrum after broadening. Figures 4–6 show the individual stick spectra for cationic states D_0 – D_3 . The strongest transitions are labeled, and the corresponding vibrational

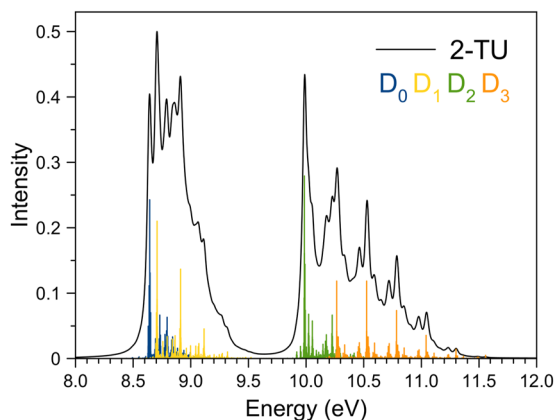


FIG. 3. Vibronic stick spectra for the lowest four transitions (from S_0 to D_0 – D_3) and the broadened spectrum for 2-TU.

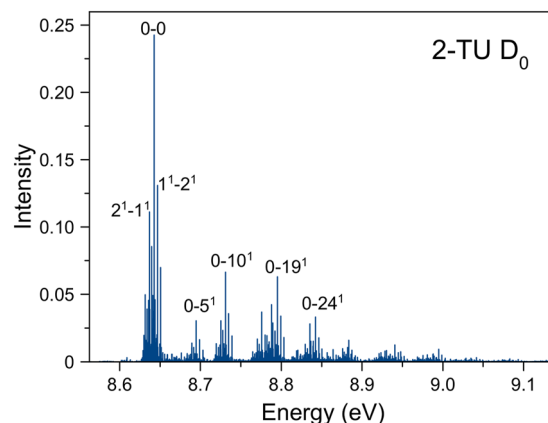


FIG. 4. $S_0 \rightarrow D_0$ stick spectrum of 2-TU with assignment of major transitions. The used notation is g^m-e^n , where g is the excited normal mode in the S_0 state, e is the excited normal mode in the D_0 state, and m and n are the numbers of vibrational quanta. “0” stands for the lowest vibrational states of S_0 and D_0 .

modes are shown in Table V. All other modes involved are shown in Tables VI–IX.

The vibronic stick spectra and the resulting electron spectrum for 4-TU are shown in Fig. 8. The individual stick spectra for cationic states D_0 – D_3 are shown in Figs. 9–12. Again, the strongest transitions are labeled, and the corresponding modes are shown in Table X. All other modes involved are shown in Tables XI–XIV.

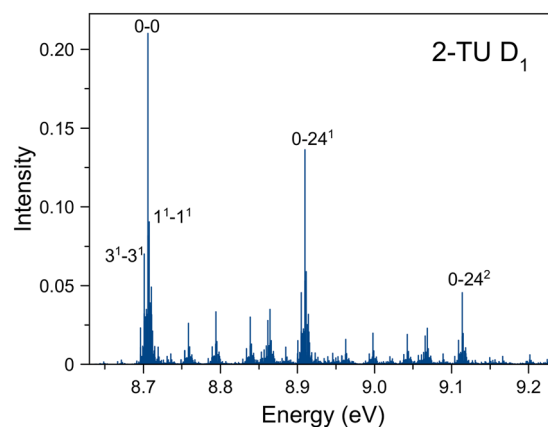


FIG. 5. $S_0 \rightarrow D_1$ stick spectrum of 2-TU with assignment of major transitions. The used notation is g^m-e^n , where g is the excited normal mode in the S_0 state, e is the excited normal mode in the D_1 state, and m and n are the numbers of vibrational quanta. “0” stands for the lowest vibrational states of S_0 and D_1 .

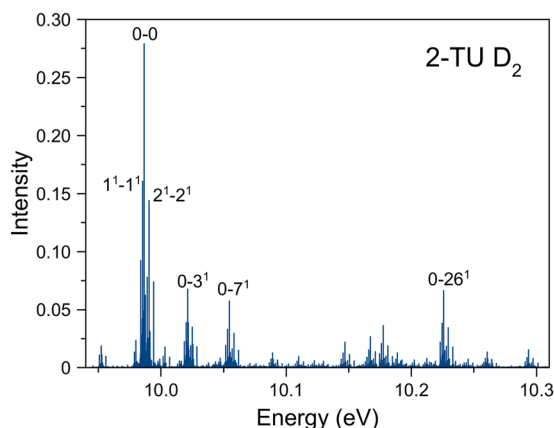


FIG. 6. $S_0 \rightarrow D_2$ stick spectrum of 2-TU with assignment of major transitions. The used notation is g^m-e^n , where g is the excited normal mode in the S_0 state, e is the excited normal mode in the D_2 state, and m and n are the numbers of vibrational quanta. "0" stands for the lowest vibrational states of S_0 and D_2 .

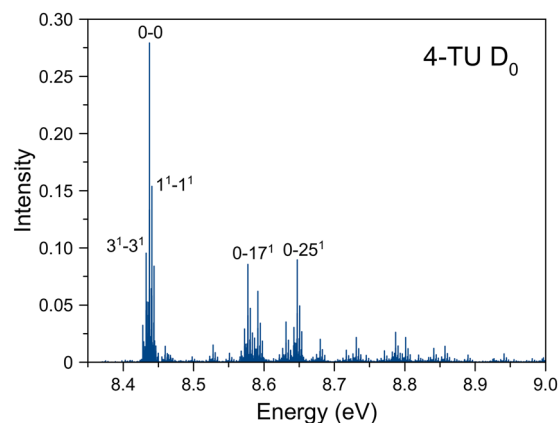


FIG. 9. $S_0 \rightarrow D_0$ stick spectrum of 4-TU with assignment of major transitions. The used notation is g^m-e^n , where g is the excited normal mode in the S_0 state, e is the excited normal mode in the D_0 state, and m and n are the numbers of vibrational quanta. "0" stands for the lowest vibrational states of S_0 and D_0 .

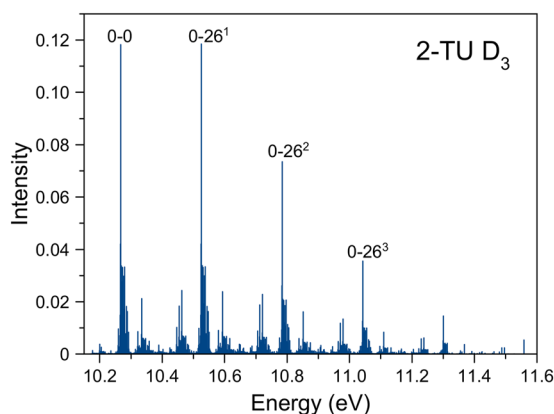


FIG. 7. $S_0 \rightarrow D_3$ stick spectrum of 2-TU with assignment of major transitions. The used notation is g^m-e^n , where g is the excited normal mode in the S_0 state, e is the excited normal mode in the D_3 state, and m and n are the numbers of vibrational quanta. "0" stands for the lowest vibrational states of S_0 and D_3 .

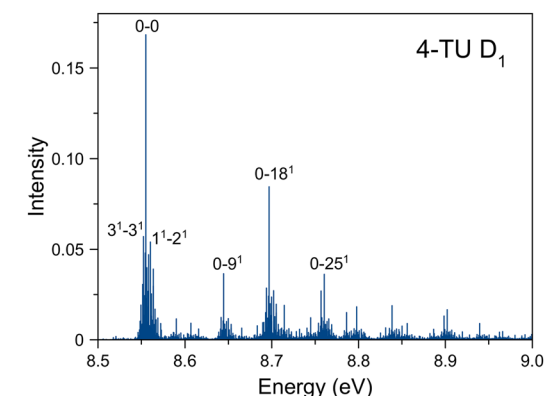


FIG. 10. $S_0 \rightarrow D_1$ stick spectrum of 4-TU with assignment of major transitions. The used notation is g^m-e^n , where g is the excited normal mode in the S_0 state, e is the excited normal mode in the D_1 state, and m and n are the numbers of vibrational quanta. "0" stands for the lowest vibrational states of S_0 and D_1 .

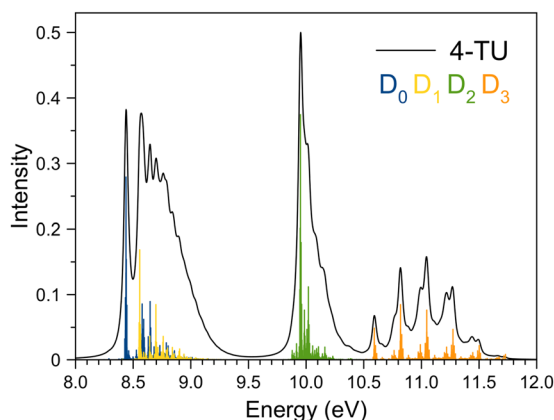


FIG. 8. Vibronic stick spectra for the lowest four transitions (from S_0 to D_0 - D_3) and the broadened spectrum for 4-TU.

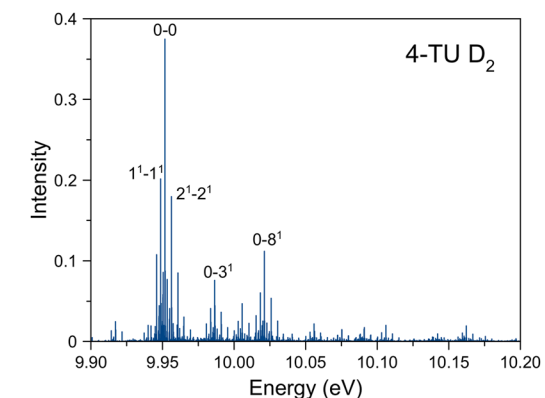


FIG. 11. $S_0 \rightarrow D_2$ stick spectrum of 4-TU with assignment of major transitions. The used notation is g^m-e^n , where g is the excited normal mode in the S_0 state, e is the excited normal mode in the D_2 state, and m and n are the numbers of vibrational quanta. "0" stands for the lowest vibrational states of S_0 and D_2 .

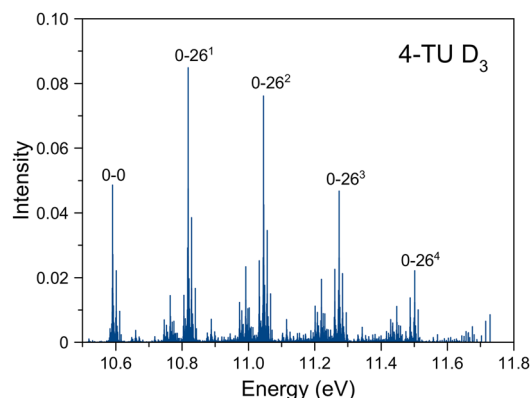


FIG. 12. $S_0 \rightarrow D_3$ stick spectrum of 4-TU with assignment of major transitions. The used notation is g^m-e^n , where g is the excited normal mode in the S_0 state, e is the excited normal mode in the D_3 state, and m and n are the numbers of vibrational quanta. “0” stands for the lowest vibrational states of S_0 and D_3 .

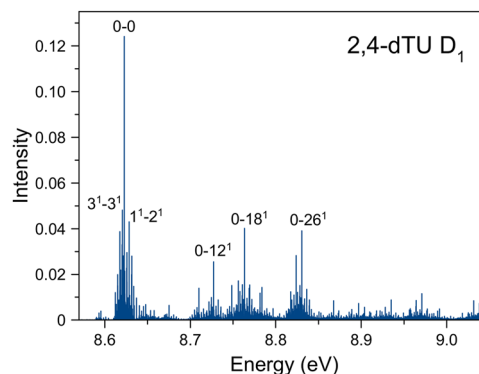


FIG. 15. $S_0 \rightarrow D_1$ stick spectrum of 2,4-dTU with assignment of major transitions. The used notation is g^m-e^n , where g is the excited normal mode in the S_0 state, e is the excited normal mode in the D_1 state, and m and n are the numbers of vibrational quanta. “0” stands for the lowest vibrational states of S_0 and D_1 .

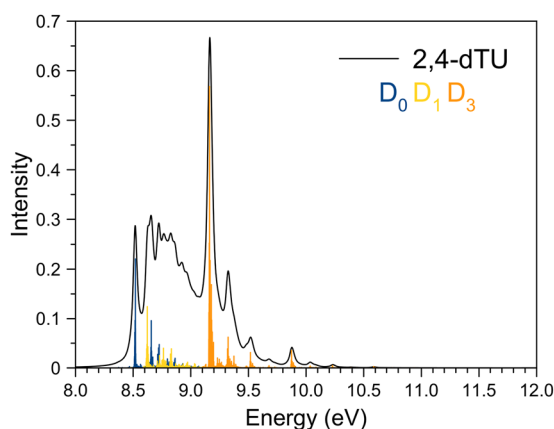


FIG. 13. Vibronic stick spectra for the transitions from S_0 to D_0 , D_1 , and D_3 and the broadened spectrum for 2,4-dTU.

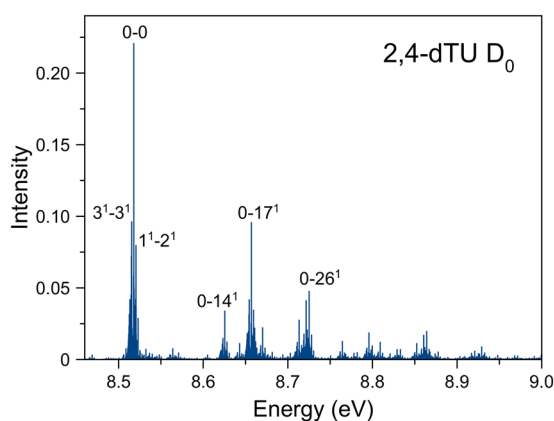


FIG. 14. $S_0 \rightarrow D_0$ stick spectrum of 2,4-dTU with assignment of major transitions. The used notation is g^m-e^n , where g is the excited normal mode in the S_0 state, e is the excited normal mode in the D_0 state, and m and n are the numbers of vibrational quanta. “0” stands for the lowest vibrational states of S_0 and D_0 .

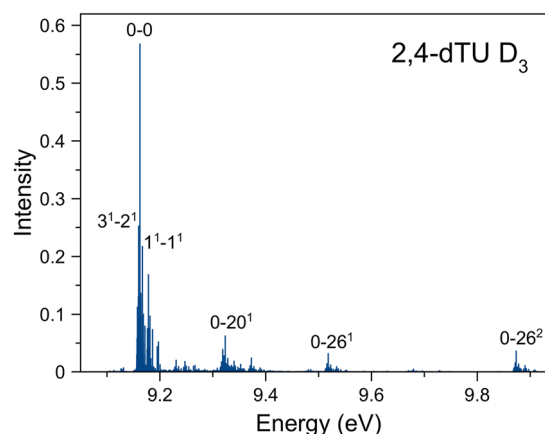


FIG. 16. $S_0 \rightarrow D_3$ stick spectrum of 2,4-dTU with assignment of major transitions. The used notation is g^m-e^n , where g is the excited normal mode in the S_0 state, e is the excited normal mode in the D_3 state, and m and n are the numbers of vibrational quanta. “0” stands for the lowest vibrational states of S_0 and D_3 .

TABLE V. S_0 normal modes of 2-TU involved in the major vibronic transitions from S_0 to D_0 – D_3 .

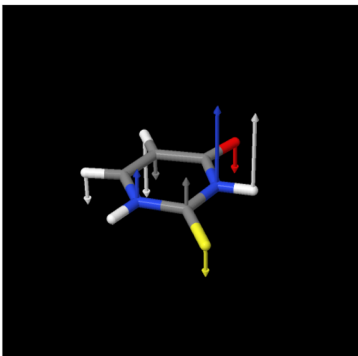
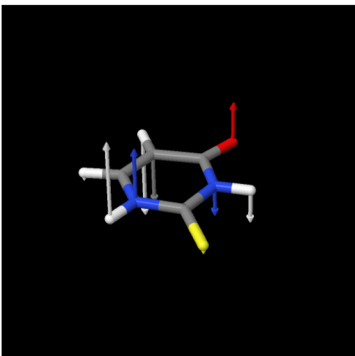
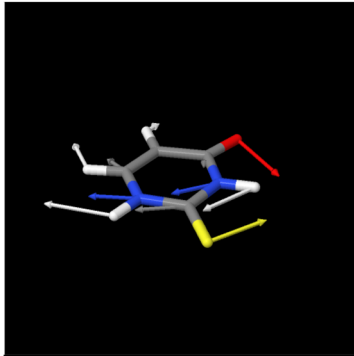
2-TU S_0		
		
mode 1, 119 cm^{-1}	mode 2, 188 cm^{-1}	mode 3, 280 cm^{-1}

TABLE VI. D_0 normal modes of 2-TU involved in the major $S_0 \rightarrow D_0$ vibronic transitions.

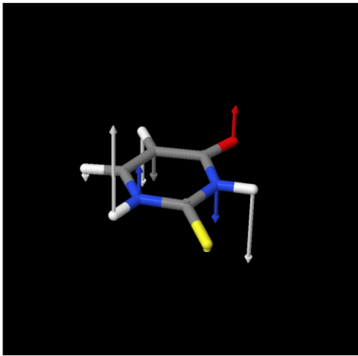
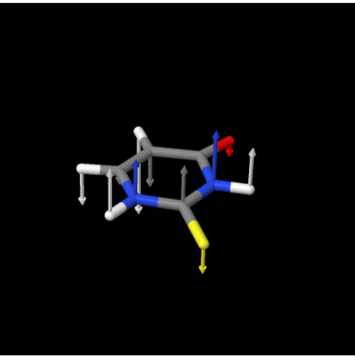
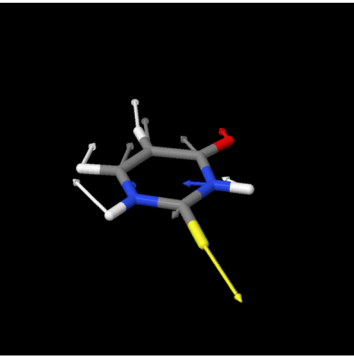
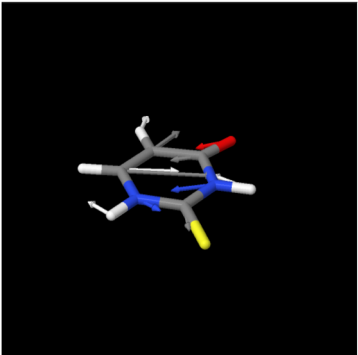
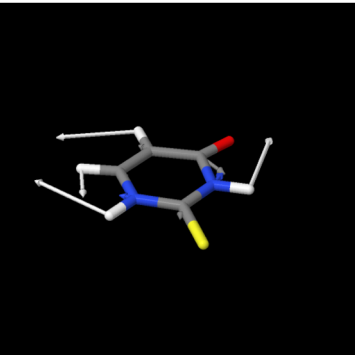
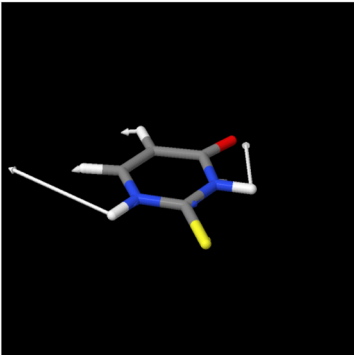
2-TU D_0		
		
mode 1, 112 cm^{-1}	mode 2, 163 cm^{-1}	mode 5, 420 cm^{-1}
		
mode 10, 711 cm^{-1}	mode 19, 1231 cm^{-1}	mode 24, 1609 cm^{-1}

TABLE VII. D_1 normal modes of 2-TU involved in the major $S_0 \rightarrow D_1$ vibronic transitions.

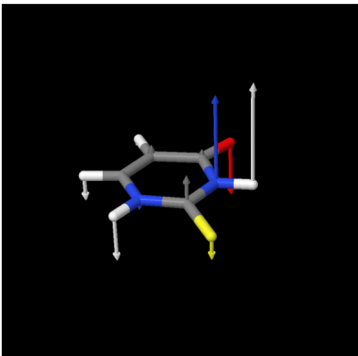
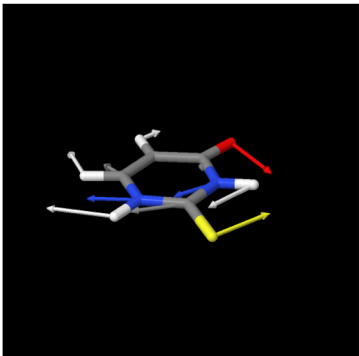
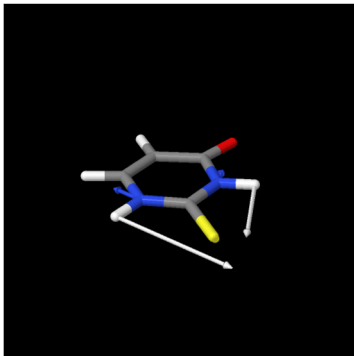
2-TU D_1		
		
mode 1, 141 cm^{-1}	mode 3, 238 cm^{-1}	mode 24, 1645 cm^{-1}

TABLE VIII. D_2 normal modes of 2-TU involved in the major $S_0 \rightarrow D_2$ vibronic transitions.

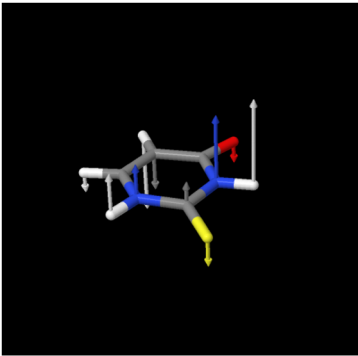
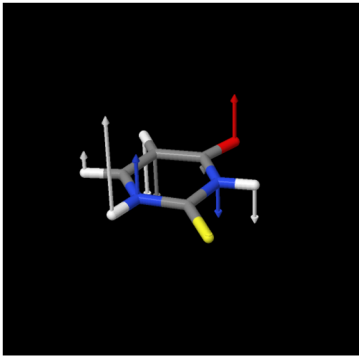
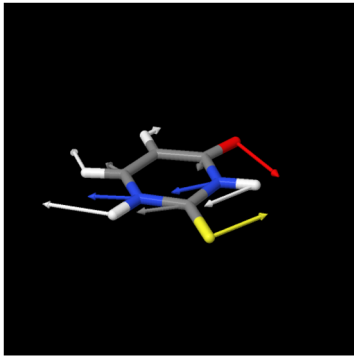
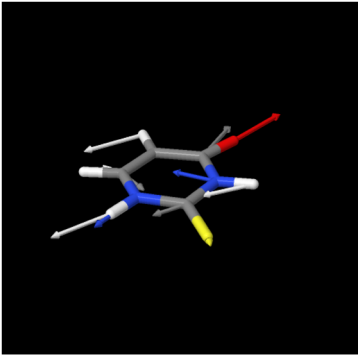
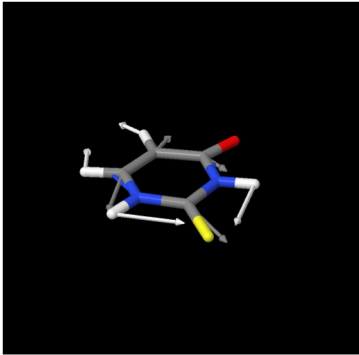
2-TU D_2		
		
mode 1, 119 cm^{-1}	mode 2, 188 cm^{-1}	mode 3, 280 cm^{-1}
		
mode 7, 548 cm^{-1}	mode 26, 1929 cm^{-1}	

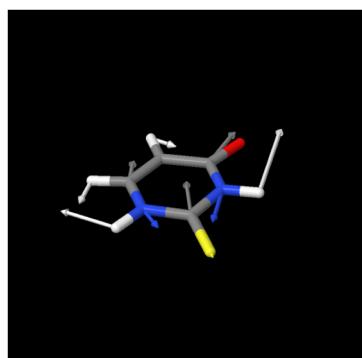
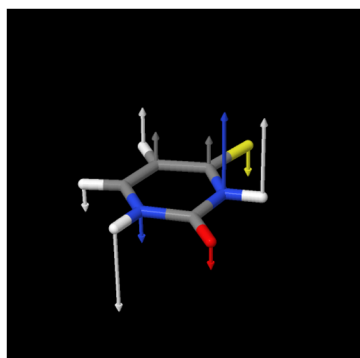
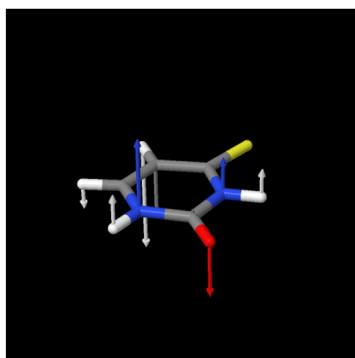
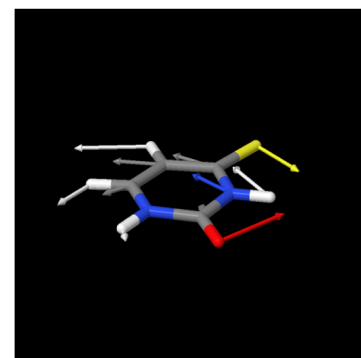
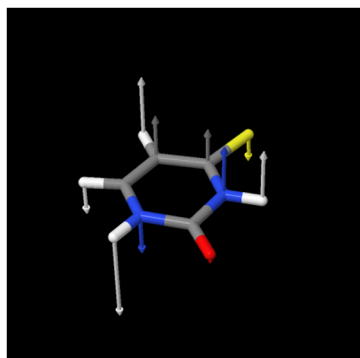
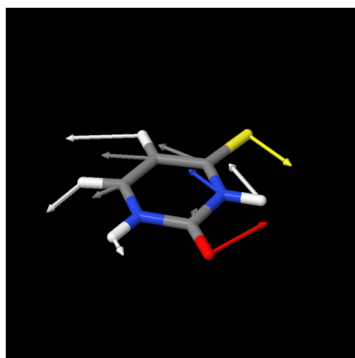
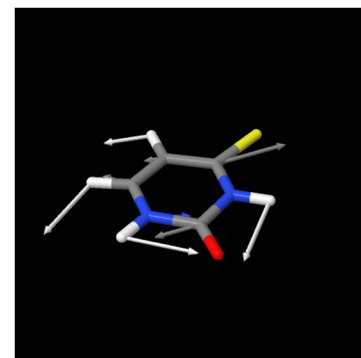
TABLE IX. D_3 normal modes of 2-TU involved in the major $S_0 \rightarrow D_3$ vibronic transitions.2-TU D_3 mode 26, 2083 cm^{-1} **TABLE X.** S_0 normal modes of 4-TU involved in the major vibronic transitions from S_0 to D_0 – D_3 .4-TU S_0 mode 1, 126 cm^{-1} mode 2, 158 cm^{-1} mode 3, 279 cm^{-1} **TABLE XI.** D_0 normal modes of 4-TU involved in the major $S_0 \rightarrow D_0$ vibronic transitions.4-TU D_0 mode 1, 153 cm^{-1} mode 3, 240 cm^{-1} mode 17, 1128 cm^{-1}

TABLE XI. (Continued.)

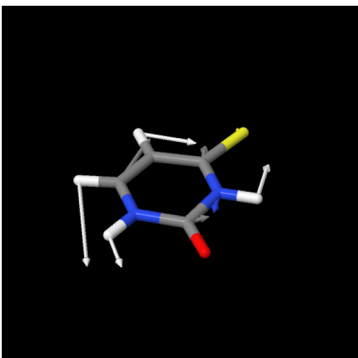
4-TU D ₀

mode 25, 1692 cm ⁻¹

TABLE XII. D₁ normal modes of 4-TU involved in the major S₀ → D₁ vibronic transitions.

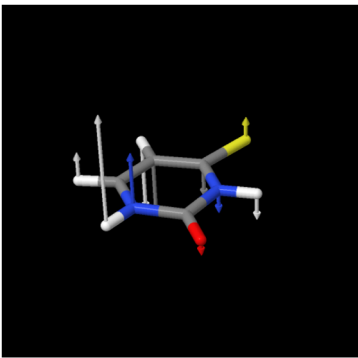
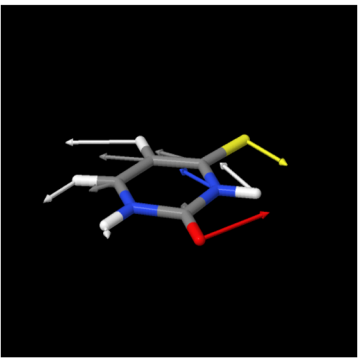
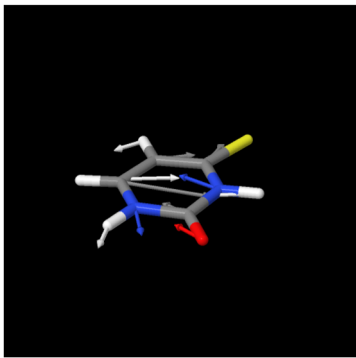
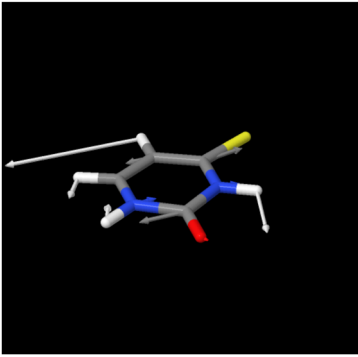
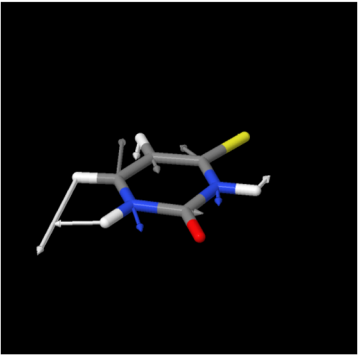
4-TU D ₁		
		
mode 2, 169 cm ⁻¹	mode 3, 256 cm ⁻¹	mode 9, 722 cm ⁻¹
		
mode 18, 1143 cm ⁻¹	mode 25, 1657 cm ⁻¹	

TABLE XIII. D_2 normal modes of 4-TU involved in the major $S_0 \rightarrow D_2$ vibronic transitions.

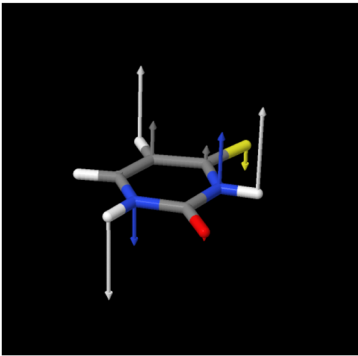
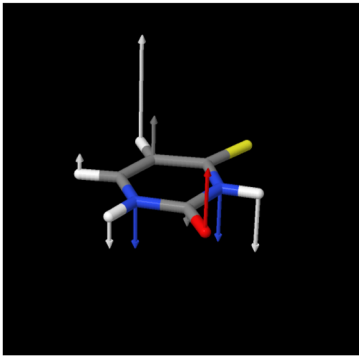
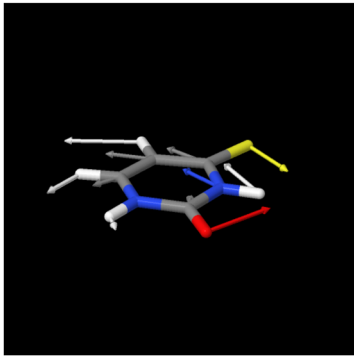
4-TU D_2		
		
mode 1, 103 cm^{-1}	mode 2, 195 cm^{-1}	mode 3, 281 cm^{-1}

TABLE XIII. (Continued.)

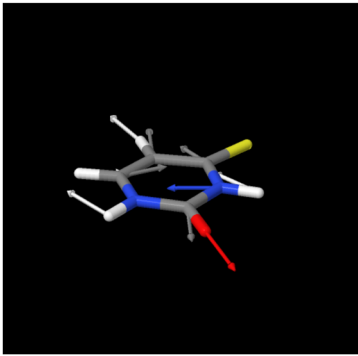
4-TU D_2

mode 8, 561 cm^{-1}

TABLE XIV. D_3 normal modes of 4-TU involved in the major $S_0 \rightarrow D_3$ vibronic transitions.

4-TU D_3

mode 26, 1836 cm^{-1}

TABLE XV. S_0 normal modes of 2,4-dTU involved in the major vibronic transitions from S_0 to D_0 , D_1 , and D_3 .

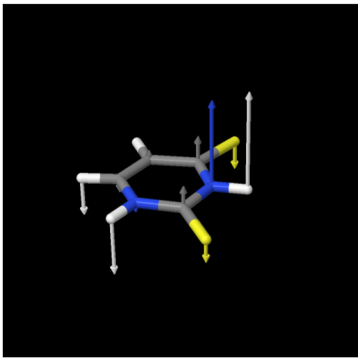
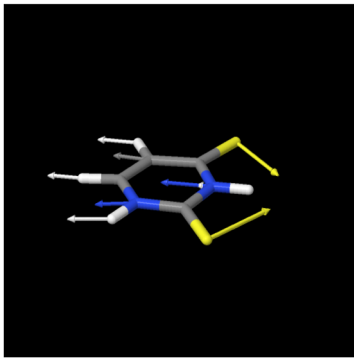
2,4-dTU S_0	
	
mode 1, 123 cm^{-1}	mode 3, 220 cm^{-1}

TABLE XVI. D_0 normal modes of 2,4-dTU involved in the major $S_0 \rightarrow D_0$ vibronic transitions.

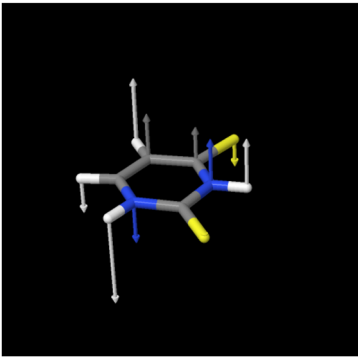
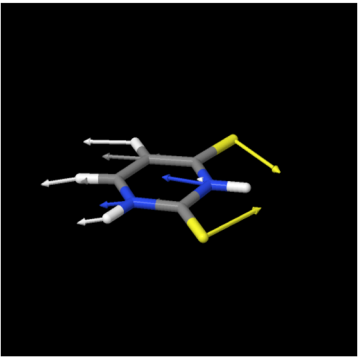
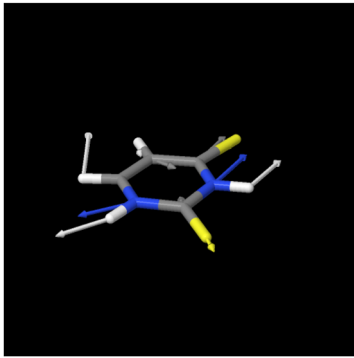


2,4-dTU D_0		
		
mode 2, 144 cm^{-1}	mode 3, 201 cm^{-1}	mode 14, 868 cm^{-1}
		
mode 17, 1121 cm^{-1}	mode 26, 1673 cm^{-1}	

TABLE XVII. D_1 normal modes of 2,4-dTU involved in the major $S_0 \rightarrow D_1$ vibronic transitions.

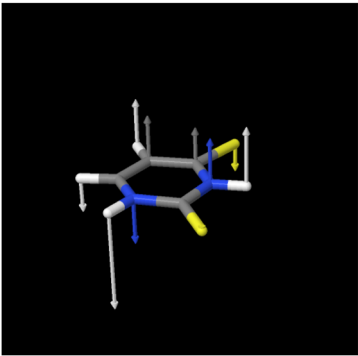
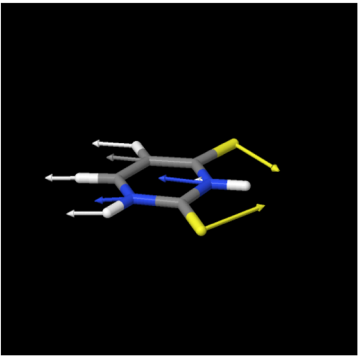
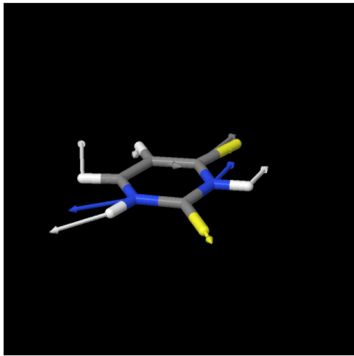
2,4-dTU D_1		
		
mode 2, 168 cm^{-1}	mode 3, 201 cm^{-1}	mode 12, 841 cm^{-1}

TABLE XVII. (Continued.)

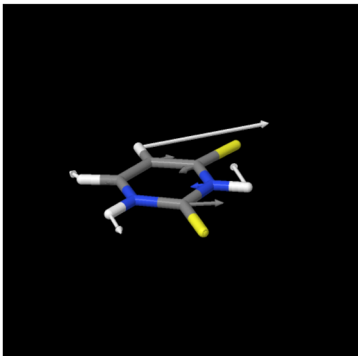
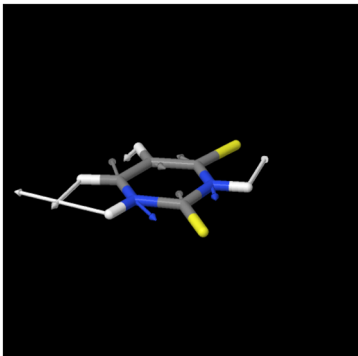
2,4-dTU D_1	
	
mode 18, 1133 cm^{-1}	mode 26, 1676 cm^{-1}

TABLE XVIII. D_3 normal modes of 2,4-dTU involved in the major $S_0 \rightarrow D_3$ vibronic transitions.


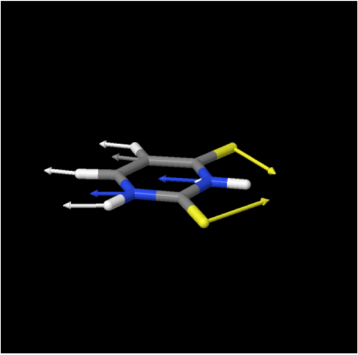
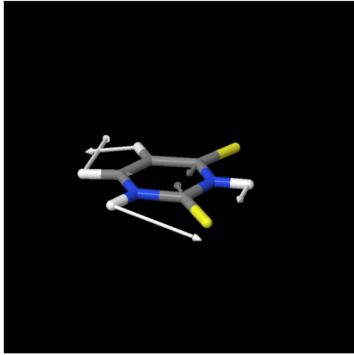
2,4-dTU D_3		
		
mode 1, 162 cm^{-1}	mode 2, 202 cm^{-1}	mode 20, 1304 cm^{-1}

TABLE XVIII. (Continued.)

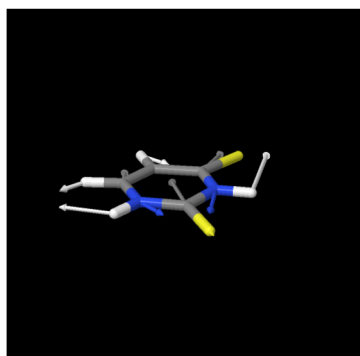
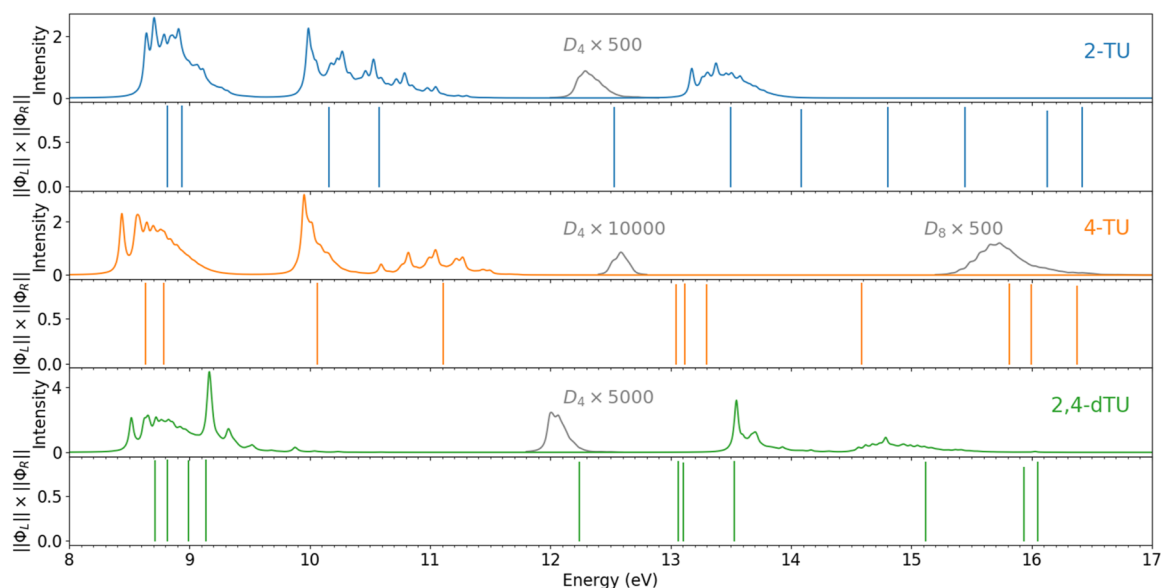
2,4-dTU D₃mode 26, 2872 cm⁻¹

FIG. 17. Calculated spectra with amplified weak transitions shown in gray.

APPENDIX B: CALCULATED WEAK TRANSITIONS

Figure 17 shows again the calculated spectra for the thiouracils. In addition, the weak transitions to cationic states D₄ and D₈ were scaled and plotted in gray. The scaling factor is given in gray labels.

REFERENCES

- ¹S. Arslançan, L. Martínez-Fernández, and I. Corral, “Photophysics and photochemistry of canonical nucleobases’ thioanalogs: From quantum mechanical studies to time resolved experiments,” *Molecules* **22**(6), 998 (2017).
- ²B. Ashwood, M. Pollum, and C. E. Crespo-Hernández, “Photochemical and photodynamical properties of sulfur-substituted nucleic acid bases,” *Photochem. Photobiol.* **95**(1), 33–58 (2019).
- ³R. Brem and P. Karran, “Multiple forms of DNA damage caused by UVA photoactivation of DNA 6-thioguanine,” *Photochem. Photobiol.* **88**(1), 5–13 (2012).
- ⁴L. A. Ortiz-Rodríguez and C. E. Crespo-Hernández, “Thionated organic compounds as emerging heavy-atom-free photodynamic therapy agents,” *Chem. Sci.* **11**(41), 11113–11123 (2020).
- ⁵M. Pollum, S. Jockusch, and C. E. Crespo-Hernández, “Increase in the photoreactivity of uracil derivatives by doubling thionation,” *Phys. Chem. Chem. Phys.* **17**(41), 27851–27861 (2015).
- ⁶R. Borrego-Varillas, D. C. Teles-Ferreira, A. Nenov, I. Conti, L. Ganzer, C. Manzoni, M. Garavelli, A. Maria de Paula, and G. Cerullo, “Observation of the sub-100 femtosecond population of a dark state in a thio base mediating intersystem crossing,” *J. Am. Chem. Soc.* **140**(47), 16087–16093 (2018).

- ⁷D. C. Teles-Ferreira, I. Conti, R. Borrego-Varillas, A. Nenov, I. H. M. Van Stokkum, L. Ganzer, C. Manzoni, A. M. de Paula, G. Cerullo, and M. Garavelli, "A unified experimental/theoretical description of the ultrafast photo-physics of single and double thionated uracils," *Chem.-Eur. J.* **26**(1), 336–343 (2020).
- ⁸D. C. Teles-Ferreira, I. H. van Stokkum, I. Conti, L. Ganzer, C. Manzoni, M. Garavelli, G. Cerullo, A. Nenov, R. Borrego-Varillas, and A. M. de Paula, "Coherent vibrational modes promote the ultrafast internal conversion and intersystem crossing in thiobases," *Phys. Chem. Chem. Phys.* **24**(36), 21750–21758 (2022).
- ⁹J. A. Sánchez-Rodríguez, A. Mohamadze, S. Mai, B. Ashwood, M. Pollum, P. Marquetand, L. González, C. E. Crespo-Hernández, and S. Ullrich, "2-thiouracil intersystem crossing photodynamics studied by wavelength-dependent photoelectron and transient absorption spectroscopies," *Phys. Chem. Chem. Phys.* **19**(30), 19756–19766 (2017).
- ¹⁰M. S. Robinson, M. Niebuhr, and M. Gühr, "Ultrafast photo-ion probing of the relaxation dynamics in 2-thiouracil," *Molecules* **28**(5), 2354 (2023).
- ¹¹A. Mohamadze, S. Bai, M. Barbatti, and S. Ullrich, "Intersystem crossing dynamics in singly substituted thiouracil studied by time-resolved photoelectron spectroscopy: Micro-environmental effects due to sulfur position," *Chem. Phys.* **515**, 572–579 (2018).
- ¹²A. Mohamadze and S. Ullrich, "Internal conversion and intersystem crossing dynamics of uracil upon double thionation: A time-resolved photoelectron spectroscopy study in the gas phase," *Phys. Chem. Chem. Phys.* **22**(27), 15608–15615 (2020).
- ¹³F. Lever, D. Mayer, D. Picconi, J. Metje, S. Alisauskas, F. Calegari, S. Düsterer, C. Ehlert, R. Feifel, M. Niebuhr, B. Manschwetus, M. Kuhlmann, T. Mazza, M. S. Robinson, R. J. Squibb, A. Trabattini, M. Wallner, P. Saalfrank, T. J. A. Wolf, and M. Gühr, "Ultrafast dynamics of 2-thiouracil investigated by time-resolved Auger spectroscopy," *J. Phys. B: At., Mol. Opt. Phys.* **54**(1), 014002 (2020).
- ¹⁴D. Mayer, F. Lever, D. Picconi, J. Metje, S. Alisauskas, F. Calegari, S. Düsterer, C. Ehlert, R. Feifel, M. Niebuhr, B. Manschwetus, M. Kuhlmann, T. Mazza, M. S. Robinson, R. J. Squibb, A. Trabattini, M. Wallner, P. Saalfrank, T. J. A. Wolf, and M. Gühr, "Following excited-state chemical shifts in molecular ultrafast x-ray photoelectron spectroscopy," *Nat. Commun.* **13**(1), 198 (2022).
- ¹⁵F. Lever, D. Picconi, D. Mayer, S. Alisauskas, F. Calegari, S. Düsterer, R. Feifel, M. Kuhlmann, T. Mazza, J. Metje, M. S. Robinson, R. J. Squibb, A. Trabattini, M. Ware, P. Saalfrank, T. J. A. Wolf, and M. Gühr, "Direct observation of the $\pi\pi^*$ to $n\pi^*$ transition in 2-thiouracil via time-resolved NEXAFS spectroscopy," *J. Phys. Chem. Lett.* **16**(16), 4038–4046 (2025).
- ¹⁶D. Mayer, D. Picconi, M. S. Robinson, and M. Gühr, "Experimental and theoretical gas-phase absorption spectra of thionated uracils," *Chem. Phys.* **558**, 111500 (2022).
- ¹⁷D. Mayer, M. Handrich, D. Picconi, F. Lever, L. Mehner, M. L. Murillo-Sánchez, C. Walz, E. Titov, J. Bozek, P. Saalfrank, and M. Gühr, "X-ray photoelectron and NEXAFS spectroscopy of thionated uracils in the gas phase," *J. Chem. Phys.* **161**, 134301 (2024).
- ¹⁸M. Ruckebauer, S. Mai, P. Marquetand, and L. González, "Photoelectron spectra of 2-thiouracil, 4-thiouracil, and 2,4-dithiouracil," *J. Chem. Phys.* **144**(7), 074303 (2016).
- ¹⁹See <https://www.synchrotron-soleil.fr/en/beamlines/pleiades> for a description of the PLEIADES beamline at SOLEIL.
- ²⁰M. A. V. Ribeiro da Silva, L. M. P. F. Amaral, and P. Szterner, "Experimental study on the thermochemistry of 2-thiouracil, 5-methyl-2-thiouracil and 6-methyl-2-thiouracil," *J. Chem. Thermodyn.* **57**, 380–386 (2013).
- ²¹G. D. Purvis III and R. J. Bartlett, "A full coupled-cluster singles and doubles model: The inclusion of disconnected triples," *J. Chem. Phys.* **76**, 1910–1918 (1982).
- ²²D. Sinha, S. K. Mukhopadhyay, R. Chaudhuri, and D. Mukherjee, "The eigenvalue-independent partitioning technique in Fock space: An alternative route to open-shell coupled-cluster theory for incomplete model spaces," *Chem. Phys. Lett.* **154**(6), 544–549 (1989).
- ²³J. F. Stanton and J. Gauss, "Analytic energy derivatives for ionized states described by the equation-of-motion coupled cluster method," *J. Chem. Phys.* **101**, 8938–8944 (1994).
- ²⁴W. J. Hehre, R. Ditchfield, and J. A. Pople, "Self-Consistent molecular orbital methods. XII. Further extensions of Gaussian-Type basis sets for use in molecular orbital studies of organic molecules," *J. Chem. Phys.* **56**, 2257–2261 (1972).
- ²⁵P. C. Hariharan and J. A. Pople, "The influence of polarization functions on molecular orbital hydrogenation energies," *Theor. Chim. Acta* **28**, 213–222 (1973).
- ²⁶M. M. Francl, W. J. Pietro, W. J. Hehre, J. S. Binkley, M. S. Gordon, D. J. DeFrees, and J. A. Pople, "Self-consistent molecular orbital methods. XXIII. A polarization-type basis set for second-row elements," *J. Chem. Phys.* **77**, 3654–3665 (1982).
- ²⁷T. H. Dunning, Jr., "Gaussian basis sets for use in correlated molecular calculations. I. The atoms boron through neon and hydrogen," *J. Chem. Phys.* **90**, 1007–1023 (1989).
- ²⁸D. E. Woon and T. H. Dunning, Jr., "Gaussian basis sets for use in correlated molecular calculations. III. The atoms aluminum through argon," *J. Chem. Phys.* **98**, 1358–1371 (1993).
- ²⁹Y. Shao, Z. Gan, E. Epifanovsky, A. T. B. Gilbert, M. Wormit, J. Kussmann, A. W. Lange, A. Behn, J. Deng, X. Feng, D. Ghosh, M. Goldey, P. R. Horn, L. D. Jacobson, I. Kaliman, R. Z. Khaliullin, T. Kuš, A. Landau, J. Liu, E. I. Proynov, Y. M. Rhee, R. M. Richard, M. A. Rohrdanz, R. P. Steele, E. J. Sundstrom, H. L. Woodcock, P. M. Zimmerman, D. Zuev, B. Albrecht, E. Alguire, B. Austin, G. J. O. Beran, Y. A. Bernard, E. Berquist, K. Brandhorst, K. B. Bravaya, S. T. Brown, D. Casanova, C.-M. Chang, Y. Chen, S. H. Chien, K. D. Closser, D. L. Crittenden, M. Diedenhofen, R. A. DiStasio, H. Do, A. D. Dutoi, R. G. Edgar, S. Fatehi, L. Fusti-Molnar, A. Ghysels, A. Golubeva-Zadorozhnyaya, J. Gomes, M. W. D. Hanson-Heine, P. H. P. Harbach, A. W. Hauser, E. G. Hohenstein, Z. C. Holden, T.-C. Jagau, H. Ji, B. Kaduk, K. Khistyayev, J. Kim, J. Kim, R. A. King, P. Klunzinger, D. Kosenkov, T. Kowalczyk, C. M. Krauter, K. U. Lao, A. D. Laurent, K. V. Lawler, S. V. Levchenko, C. Y. Lin, F. Liu, E. Livshits, R. C. Lochan, A. Luenser, P. Manohar, S. F. Manzer, S.-P. Mao, N. Mardirossian, A. V. Marenich, S. A. Maurer, N. J. Mayhall, E. Neuscamman, C. M. Oana, R. Olivares-Amaya, D. P. O'Neill, J. A. Parkhill, T. M. Perrine, R. Peverati, A. Prociuk, D. R. Rehn, E. Rosta, N. J. Russ, S. M. Sharada, S. Sharma, D. W. Small, A. Sodt, T. Stein, D. Stück, Y.-C. Su, A. J. W. Thom, T. Tsuchimochi, V. Vanovschi, L. Vogt, O. Vydrov, T. Wang, M. A. Watson, J. Wenzel, A. White, C. F. Williams, J. Yang, S. Yeganeh, S. R. Yost, Z.-Q. You, I. Y. Zhang, X. Zhang, Y. Zhao, B. R. Brooks, G. K. L. Chan, D. M. Chipman, C. J. Cramer, W. A. Goddard, M. S. Gordon, W. J. Hehre, A. Klamt, H. F. Schaefer, M. W. Schmidt, C. D. Sherrill, D. G. Truhlar, A. Warshel, X. Xu, A. Aspuru-Guzik, R. Baer, A. T. Bell, N. A. Besley, J.-D. Chai, A. Dreuw, B. D. Dunietz, T. R. Furlani, S. R. Gwaltney, C.-P. Hsu, Y. Jung, J. Kong, D. S. Lambrecht, W. Liang, C. Ochsenfeld, V. A. Rassolov, L. V. Slipchenko, J. E. Subotnik, T. Van Voorhis, J. M. Herbert, A. I. Krylov, P. M. W. Gill, and M. Head-Gordon, "Advances in molecular quantum chemistry contained in the Q-Chem 4 program package," *Mol. Phys.* **113**(2), 184–215 (2015).
- ³⁰S. Gozem and A. I. Krylov, "The ezSpectra suite: An easy-to-use toolkit for spectroscopy modeling," *Wiley Interdiscip. Rev.: Comput. Mol. Sci.* **12**(2), e1546 (2022).
- ³¹P. Wojcik, S. Gozem, V. Mozhaevskiy, and A. I. Krylov, <https://iopenshell.usc.edu/downloads/>.
- ³²F. Santoro and D. Jacquemin, "Going beyond the vertical approximation with time-dependent density functional theory," *Wiley Interdiscip. Rev.: Comput. Mol. Sci.* **6**(5), 460–486 (2016).
- ³³M. L. Vidal, A. I. Krylov, and S. Coriani, "Dyson orbitals within the fc-CVS-EOM-CCSD framework: Theory and application to X-ray photoelectron spectroscopy of ground and excited states," *Phys. Chem. Chem. Phys.* **22**(5), 2693–2703 (2020).
- ³⁴K. D. Fulfer, D. Hardy, A. A. Aguilar, and E. D. Poliakoff, "High-resolution photoelectron spectra of the pyrimidine-type nucleobases," *J. Chem. Phys.* **142**(22), 224310 (2015).
- ³⁵A. R. Katritzky, M. Szafran, and G. Pfister-Guillouzo, "The tautomeric equilibria of thio analogues of nucleic acid bases. Part 3. Ultraviolet photoelectron spectra

of 2-thiouracil and its methyl derivatives,” *J. Chem. Soc., Perkin Trans. 2* **2**(6), 871–876 (1990).

³⁶G. Mattioli, L. Avaldi, P. Bolognesi, A. Casavola, F. Morini, T. Van Caekenberghe, J. D. Bozek, M. C. Castrovilli, J. Chiarinelli, A. Domaracka, S. Indrajith, S. Maclot, A. R. Milosavljević, C. Nicolafrancesco, C. Nicolas, and P. Rousseau, “A study of the valence photoelectron spectrum of uracil and mixed water–uracil clusters,” *J. Chem. Phys.* **158**(11), 114301 (2023).

³⁷D. M. P. Holland, A. W. Potts, L. Karlsson, I. L. Zaytseva, A. B. Trofimov, and J. Schirmer, “A study of the valence shell electronic structure of uracil and the methyluracils,” *Chem. Phys.* **353**(1-3), 47–58 (2008).

³⁸W. Domcke and D. R. Yarkony, “Role of conical intersections in molecular spectroscopy and photoinduced chemical dynamics,” *Annu. Rev. Phys. Chem.* **63**, 325–352 (2012).

³⁹M. Assmann, H. Köppel, and S. Matsika, “Photoelectron spectrum and dynamics of the uracil cation,” *J. Phys. Chem. A* **119**(5), 866–875 (2015).

⁴⁰P. Wójcik, H. Reisler, J. F. Stanton, and A. Krylov, “Vibronic spectrum of pyrazine: New insights from multi-state-multi-mode simulations parameterized with equation-of-motion coupled-cluster methods,” *J. Chem. Phys.* **163**, 054110 (2025).